Rule-based Roof Plane Detection and Segmentation from Laser Point Clouds

Hai Huang and Claus Brenner
Institute of Cartography and Geoinformatics
Leibniz Universität Hannover
Hannover, Germany
Email: {hai.huang, claus.brenner}@ikg.uni-hannover.de

***Abstract*— This paper presents a combined bottom-up and top-down approach to 3D roof plane detection and segmentation from laser scanning point clouds. Laser scanning data of city scenes often shows noise and incompleteness because of, e.g., the clutter by trees and the reflection of windows/waterlogged depressions on the roof. Results of the bottom-up plane reconstruction may thus be limited to a number of incomplete and/or irregular regions. We proposed a joint multiple-plane detection scheme to improve the performance of the 3D Hough transform. A model-driven segmentation, which works with the constraint-rules derived from the basic roof model, is conducted to overcome the clutter and flaws in the point cloud ensuring a plausible reconstruction.**

I. Introduction

Many approaches for the reconstruction of 3D city models from measurement data have been reported in the past decades. The introduction of laser scanning makes the acquisition of 3D data easier and more accurate. Overviews are given by Brenner [1], Schnabel et al. [2] and Vosselman [3].

Recent contributions were made by Rottensteiner et al. in [4], in which an algorithm for roof line delineation is presented with a statistical framework for the determination of the needed thresholds, and Tarsha-Kurdi et al. in [5], in which they report an extended Random Sample Consensus (RANSAC) algorithm for automatic roof plane detection from airborne laser scanning data. Based on the graph description of building roofs [6], Milde et al. [7] present a formal grammar for roof plane layouts, by which means relatively complex roofs can be derived from the predefined primitives. The most recent contribution for modeling buildings with primitives is given by Oude Elberink in [8].

Building reconstruction is often based on planar surfaces, which can be obtained using different algorithms. The 3D Hough transform [9] is an application of the 2D Hough transform technique [10]. In the context of laser scanning, it is often employed for plane detection. One plane in object space can be mapped to a point in parameter space and then the mapping of all possible planes passing through a point in object space leads to a certain manifold in parameter space. The coplanar condition of multiple points can therefore be equally expressed as the intersection of their corresponding manifolds. Recently, this technique has been extended by Rabbani and Van den Heuvel [11] to more complicated primitives, e.g., cylinders.

A basic problem of automatic and reliable generation of 3D building models, however, has not been well solved. Laser scanning data taken in city scenes often shows noise and incompleteness because of clutter and occlusion, e.g., by trees, or reflection, e.g., glass windows or waterlogged depressions on the roof. Results of the conventional segmentation may therefore be limited to many incomplete and/or irregular regions. We present a combined framework for 3D building roof extraction from LIDAR data by combining the power of bottom-up and top-down approaches for the roof plane detection and segmentation. An improved 3D Hough transform is designed to find multiple planes from the point cloud at the same time. By this means a context relationship of the roof planes can be derived and utilized in the detection. We then conduct a model-driven approach to segment roofs in the found planes overcoming the flaws in laser data and ensuring regular results.

II. Joint Multiple-Plane Detection

The mostly used techniques for shape detection from point clouds are Hough transform, Region Growing, and RANSAC. No matter which technique is chosen, the plan is to find one plane each time, remove the corresponding points and go on with the next one in the next iteration. The possible problems of this scheme are: 1. time consuming search, as the remaining points are calculated repeatedly until they have been recognized and removed; 2. points that belong to two adjacent planes may be too early removed with the firstly found plane. The proposed scheme is trying to avoid these drawbacks by enhancing the Hough transform to find multiple planes at the same time. By this means the points are used more efficiently – they are calculated for only one time while being allowed to vote multiple planes.

A. 3D Hough Transform

The plane parameters, i.e., its polar coordinates, are defined as shown in Fig. 1 (left). The equation of the planes passing through the point (x, y, z) can then be expressed as

$$\rho = xcos\varphi cos\theta + ysin\varphi cos\theta + zsin\theta \qquad (1)$$

with φ the azimuth, θ the elevation, and ρ the normal distance from the origin to the plane. We define the origin to be lower than the whole point cloud so that the ranges of φ and θ can be reduced to $\varphi \in [0°, 180°]$ and $\theta \in [0°, 180°]$ considering only the upper half-sphere.

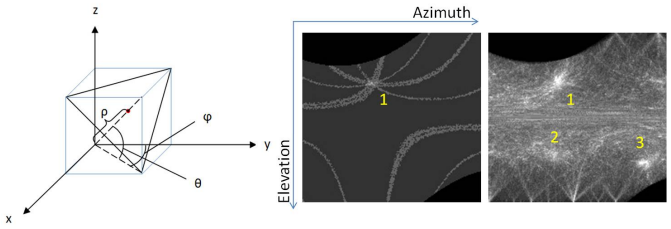

Fig. 1. Definition of the Cartesian- and polar-coordinates for the 3D Hough transform (left). 2D plots of Hough spaces for 4 points voting 1 plane (middle) and 120 points voting 3 planes (right). A lighter pixel indicates a higher manifolds concentration for the azimuth-elevation combination.

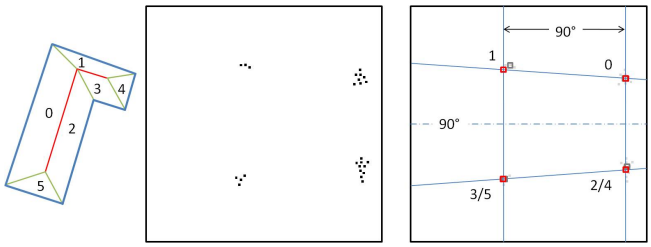

Fig. 2. Rule-based post-processing: Building model (left) with horizontal ridges (red) and diagonal ridges (green). The preliminary result from the 3D Hough transform (middle). Results before (gray) and after (red) joint planes adjustment (right).

Assuming there are n coplanar points in object space, an exclusive intersection position of their corresponding manifolds should exist in Hough space as well. In practice, however, they may not perfectly meet at one point because of the noise. On the other side, there are many trivial intersections as an arbitrary non-colinear point-triplet determines a plane. To find the best estimation of the common plane we, therefore, look for the position, in which all the corresponding manifolds show the highest degree of concentration, rather than chasing the intersected locations. To achieve this we discretize the ρ value for each φ-θ location into small intervals and use the number of manifolds passing through an interval as the measure of concentration. The size of the interval can be tuned according to the data density and quality. Mapping only the maximum concentration degree for each φ-θ location, the Hough space can be plotted into 2D, as shown in Fig. 1 (middle).

Knowing the density of the point cloud it is easy to set a threshold to accept all the potential planes. Yet, as the number of points increases, it is harder to achieve a clear result (cf. Fig. 1, right).

B. Rule-based Post-processing of the Results

The sketch in φ-θ diagram (Fig. 2, middle) demonstrates a filtered result of the 3D Hough transform showing only the locations with distinguished manifolds concentration. Although the direct result of the Hough transform is still rough, multiple planes have been recognized – top candidates of φ-θ are well concentrated in four groups. Yet, as shown in Fig. 2 (right), a simple clustering and averaging still leads to obvious errors (gray rectangles).

Assuming these planes belong to an individual building (cf. Fig. 2, left), constraints can be derived from the basic roof model to regularize the results. We subdivide the intersection lines (ridges) into two classes:

- horizontal ridges (red): ridges between two vertices on the roof;
- diagonal ridges (green): ridges connecting one vertex and one eaves corner, which include hips and valleys.

The following rules can then be derived:

1. Planes sharing a horizontal ridge have the same azimuth. E.g., for planes 0 and 2: if $|\varphi_0 - \varphi_2| < 5°$ or $> 175°$, then adjust $|\varphi_0 - \varphi_2| = 0°$ or $180°$. The variation of each φ is inversely proportional to the number of the coplanar points. This condition implies the horizontal ridge is parallel to the ground.
2. Planes sharing a horizontal ridge follow $\theta_0 + \theta_2 = 180°$ if $|\varphi_0 - \varphi_2| = 0°$ or $\theta_0 = \theta_2$ if $|\varphi_0 - \varphi_2| = 180°$, which implies that the roof has a symmetrical form.
3. Planes sharing a diagonal ridge have perpendicular azimuths. E.g., for planes 0 and 1: if $|\varphi_0 - \varphi_1| \in (90 \pm 5)°$, then force $|\varphi_0 - \varphi_1| = 90°$.

These rules work only based on the parameter values while the context (adjacency) relation of the planes is still unknown. The latter is going to be automatically derived afterwards.

The result is thereby refined as shown in Fig. 2 (right, red rectangles). Please note that this diagram only shows the distribution on azimuth-elevation, i.e., parallel planes are shown at the same position (cf. positions 3/5 and 2/4). They, however, can be easily separated by their different ρ values. Fig. 5 (b) presents the detected planes by labeling the coplanar points with different colors.

The advantage of this scheme is that the parameters of multiple planes are jointly adjusted, i.e., points of multiple planes contribute to their common parameter, e.g., azimuth of planes 0 and 2, making the result more accurate and reasonable.

C. Relation Matrix and Region Adjacency Graph

Intersection lines are calculated after the planes have been detected. We count points that belong to (the vicinity of) the intersection lines and note the numbers down in a relation matrix (Fig. 3, middle). Yet, as both the planes and the intersection lines are infinite before the segmentation (cf. Section III), false intersections, e.g., planes 0-3 and planes 1-2 (gray dashed lines in Fig. 3, left), could still be found. We verify the intersection lines by checking the plane normal vectors on its both sides: if the vectors are similar to each other, the intersection is false and the corresponding number in the matrix cell is set to null.

Please note that the relation matrix is symmetric and we use the lower triangle (gray) to show the initial values while the upper triangle (color, italic) presenting the result after the verification of intersections. Drawing all non-zero relations shown in the matrix results in a Region Adjacency Graph

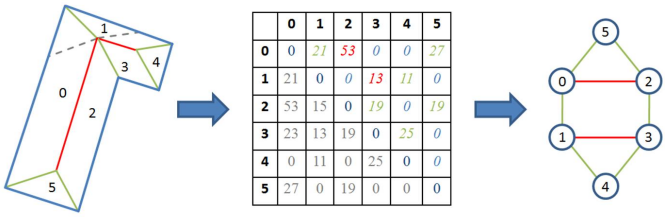

Fig. 3. Relation matrix (middle) is generated by analyzing intersection lines (left) and leads to a RAG (right). Intersection lines are verified to eliminate the false ones (gray dashed lines).

(RAG, Fig. 3, right), where the two classes of ridges are shown in red and green colors respectively.

III. Plane Segmentation

After the plane parameters and the intersection lines have been determined, the plane segmentation means finding the ridges, i.e., to segment the intersection lines, and eaves, i.e., to find the lower edges of the roof planes.

A. Ridge Determination

A ridge is a segment of an intersection line. As mentioned in Section II-B, a horizontal ridge (red) has both end points at vertices. Studying the RAG, we can see that each basic closed circle (e.g., 0-2-5 or 0-1-3-2) indicates a vertex on the roof (cf. Fig. 3):

$$v_{0-2-5} = P_0 \cap P_2 \cap P_5 = r_{0-2} \cap P_5 \; ; \tag{2}$$

$$v_{0-1-3-2} = P_0 \cap P_1 \cap P_3 \cap P_2 = r_{0-2} \cap r_{1-3} \tag{3}$$

with v_{m-n-p} the vertex of plane $m-n-p$, P_n the plane n, and r_{m-n} the ridge connecting plane $m-n$. The diagonal ridges will be finished after the determination of eaves.

B. Edge Sweeping for Eaves

An improved edge sweeping is conducted to find the eave lines. It works based on Maximum a Posteriori (MAP) estimation of the eave parameters. As the planes and horizontal ridges are already known, the parameters of eaves, which are coplanar with the corresponding ridge, can be simplified as $\Theta = \{d, \alpha\}$ with d the sweeping distance and α the angle on the common plane. The sweeping distance is defined as the normal distance from the midpoint/endpoint (cf. e.g., P_0/P_5) of the ridge to the eave.

We use the following constraints as prior information:

1. Eaves are parallel (e.g., P_0) or perpendicular (e.g., P_5) to the horizontal ridge:

$$p(\alpha_{eave}) = N(\alpha_{hridge}, \sigma_\alpha^2) \; or \; N(\alpha_{hridge} + \frac{\Pi}{2}, \sigma_\alpha^2) \; . \tag{4}$$

2. Symmetry of eaves to both sides of the horizontal ridge:

$$p(|d - d'|) = N(0, \sigma_d^2) \tag{5}$$

with d and d' the sweeping distances of both sides of the ridge. It can be controlled by tuning σ_d and even be overruled if the numbers of found points on both sides are very different.

Quality of reconstruction is employed as the likelihood function – the goodness of fit of the underlying model (generated by the sampling of Θ) to the data.

$$L(\mathcal{D}|\Theta) = Quality = \frac{TP}{TP + FP + FN} \tag{6}$$

with $\mathcal{D}$ the data, i.e., the point cloud and

- TP: True Positive, plane points which have been included inside the eave;
- FP: False Positive, plane points outside the eave;
- FN: False Negative, the included position has no point in the roof plane (for point raster).

Integrating the prior information in the objective function, the MAP estimation of the eave parameters can then be expressed as:

$$\widehat{\Theta}_{MAP} = \underset{\Theta}{argmax} \left\{ \frac{L(\mathcal{D}|\Theta)p(\Theta)}{P(\mathcal{D})} \right\} = \underset{\Theta}{argmax} \left\{ L(\mathcal{D}|\Theta)p(\Theta) \right\} \tag{7}$$

with $p(\Theta) = p(\alpha) \cdot p(|d - d'|)$ and $P(\mathcal{D})$ the marginal probability. $P(\mathcal{D})$ can be seen as a constant in the optimization, as it does not depend on Θ.

Fig. 4 demonstrates how the proposed rule-based edge sweeping works. Eaves parallel to the ridge are searched jointly with the consideration of the parallelism and the symmetry – first sweeping one eave by increasing d from the horizontal ridge and then sampling d' from $p(|d-d'|)$ as well as α from $p(\alpha)$ in each d-step. This helps to sort out the points caused by the tree clutter (on both sides, cf. also Fig. 5) and to compensate the missing points (on the right side). Eaves perpendicular to the ridge are found holding the angle constraint.

The rules used in the edge sweeping are derived from a simplified gable roof model. They are, as in (4) and (5), relaxed to gain more flexibility in the reconstruction.

IV. Results

Fig. 5 shows a result of the proposed approach. The raw point cloud (Fig. 5, a) has relatively low density (1 meter raster) and the roof points (blue solid polygon) are cluttered by

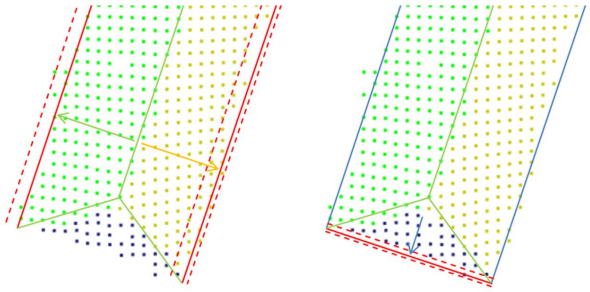

Fig. 4. Rule-based edge sweeping of the eaves parallel (left) and perpendicular (right) to the horizontal ridge.

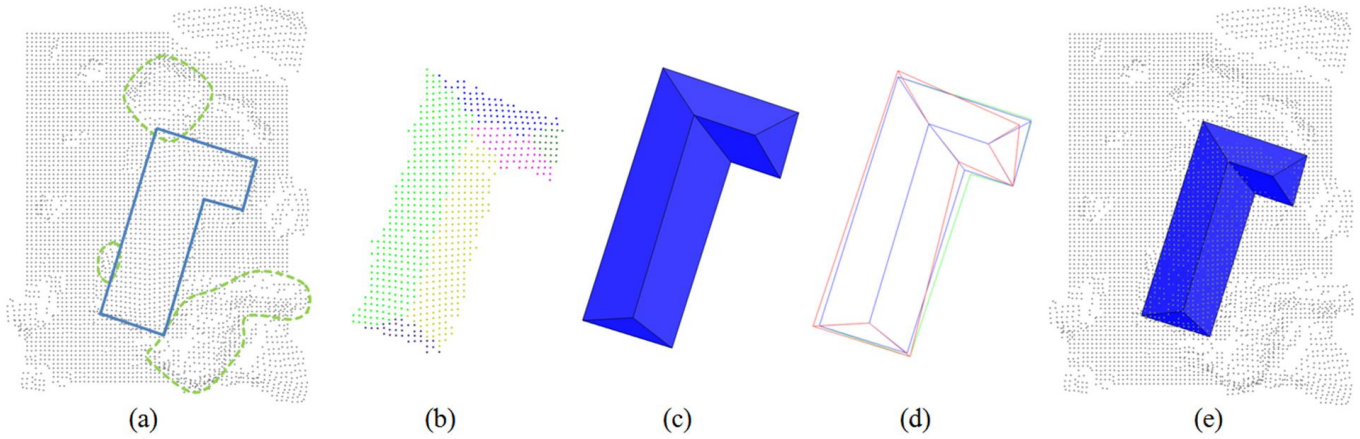

Fig. 5. Experimental result: (a) In the raw point cloud the roof (blue solid polygon) is cluttered by several trees (green dashed contours). (b) Some adjacent tree points are falsely labeled as roof points in the plane detection. (c) The rule-based segmentation ensures the regularity of the roof. (d) The comparison of results of simple bottom-up (red) and rule-based (blue) reconstructions with the building footprint (green). (e) The final roof model in the point cloud.

several adjacent trees (green dashed contours). Their influence remains in the simple bottom-up segmentation because some tree points have been falsely labeled as roof points after the plane detection (Fig. 5, b). This difficulty, as mentioned in Section III-B, is overcome by the rule-based segmentation (Fig. 5, c). We compare the simple bottom-up reconstruction (red) and our result (blue) with the building footprint data (green) in Fig. 5 (d), the integration of model-driven approach has notably improved the result. Fig. 5 (e) presents the final roof model fitting the point cloud.

Please note although the reconstructed eave contour is close to the building footprint, they should in principle not be identical, as the latter is measured based on the wall/wainscot. The result shows good correctness by being well parallel to the corresponding lines in the footprint rather than matching them.

V. Conclusion and Outlook

This paper presents an approach to 3D detection and segmentation of building roof planes combining bottom-up and top-down methods. The main contributions can be concluded as follows:

1. A joint multiple-plane detection scheme is proposed to enhance the result of 3D Hough transform.
2. A model-driven segmentation is conducted by integrating model constraints into the MAP estimation of the roof parameters.

By these means the laser scanning points are used more efficiently and a plausible reconstruction is ensured.

Although we have tried to relax the search of plane parameters, the constraint rules are still limited because of the relatively simple roof models. More sophisticated models and refined rules are needed for a more flexible reconstruction.

Please note that we employ existing building footprints for the evaluation of our results. This approach, however, can be used for a reverse purpose, i.e., updating or completing building footprints derived from roof contours based on available airborne LIDAR data.

References

[1] C. Brenner, "Building reconstruction from images and laser scanning," *International Journal of Applied Earth Observation and Geoinformation, Theme Issue on Data Quality in Earth Observation Techniques*, vol. 6(3-4), pp. 187–198, 2005.

[2] R. Schnabel, R. Wessel, R. Wahl, and R. Klein, "Shape recognition in 3d point-clouds," in *The 16th International Conference in Central Europe on Computer Graphics, Visualization and Computer Vision*, 2008.

[3] G. Vosselman, "Advanced point cloud processing," in *Photogrammetric Week '09*, D. Fritsch, Ed., Heidelberg, Germany, 2009, pp. 137–146.

[4] F. Rottensteiner, J. Trinder, S. Clode, and K. Kubik, "Automated delineation of roof planes in lidar data," in *The International Archives of the Photogrammetry, Remote Sensing and Spatial Information Sciences*, vol. 36(3/W19), 2008, pp. 221–226.

[5] F. Tarsha-Kurdi, T. Landes, and P. Grussenmeyer, "Extended ransac algorithms for automatic detection of building roof plants from lidar data," *The Photogrammetric Journal of Finland*, vol. 21(1), pp. 97–109, 2008.

[6] V. Verma, R. Kumar, and S. Hsu, "3d building detection and modeling from aerial lidar data," in *The IEEE Computer Society Conference on Computer Vision and Pattern Recognition*, vol. 2, 2006, pp. 2213–2220.

[7] J. Milde, Y. Zhang, C. Brenner, L. Plümer, and M. Sester, "Building reconstruction using a structural description based on a formal grammar," in *The International Archives of the Photogrammetry, Remote Sensing and Spatial Information Sciences*, vol. 37, 2008, pp. 227–232.

[8] S. Oude Elberink, "Acquisition of 3d topography: automated 3d road and building reconstruction using airborne laser scanner data and topographic maps," Ph.D. dissertation, University of Twente, Enschede, the Netherlands, 2010.

[9] G. Vosselman and S. Dijkman, "3d building model reconstruction from point clouds and ground plans," in *The International Archives of the Photogrammetry, Remote Sensing and Spatial Information Sciences*, vol. 34(3/W4), 2001, pp. 37–43.

[10] P. Hough, "Method and means for recognizing complex patterns," U.S. Patent 3,069,654, 1962.

[11] T. Rabbani and F. Van den Heuvel, "Efficient Hough transform for automatic detection of cylinders in point clouds," in *ISPRS Workshop Laser Scanning*, Enschede, the Netherlands, 2005.